Inorg. Chem. **2007**, *46*, 8271–8282

Seven-Coordination versus Six-Coordination in Divalent First-Row Transition-Metal Complexes Derived from 1,10-Diaza-15-crown-5

Lea Vaiana, Martín Regueiro-Figueroa, Marta Mato-Iglesias, Carlos Platas-Iglesias, David Esteban-Gómez, Andrés de Blas,* and Teresa Rodríguez-Blas*

Departamento de Química Fundamental, Universidade da Coruña, Campus da Zapateira, Alejandro de la Sota 1, 15008 A Coruña, Spain

Received May 9, 2007

The complexes of the heptadentate receptor *N*,*N*′-bis(benzimidazol-2-ylmethyl)-1,10-diaza-15-crown-5 (**L²**) with Mn^{II}, Co^{II}, Ni^{II}, Cu^{II}, and Zn^{II} are reported. The X-ray crystal structures of the Zn^{II} and Ni^{II} complexes show that whereas the Zn^{II} ion is seven-coordinated in a (distorted) pentagonal-bipyramidal coordination environment, the Ni^{II} ion is only six-coordinated in a distorted octahedral coordination environment. Theoretical calculations on the $[M(\mathbf{L^2})]^{2+}$ systems (M = Mn, Co, Ni, Cu, or Zn) performed at the density functional theory (DFT; B3LYP) level have been used to obtain information about the structure and electronic properties of these complexes, as well as to rationalize their preferences for a pentagonal-bipyramidal or an octahedral coordination. We have found that for the Mn^{II}, Co^{II}, Cu^{II}, and Zn^{II} complexes, geometry optimizations lead systematically to pentagonal-bipyramidal coordination environments around the metal ions. However, for the Ni^{II} complex, two minimum-energy conformations were obtained, with the metal ion being in octahedral (*o*-$[Ni(\mathbf{L^2})]^{2+}$) or pentagonal-bipyramidal (*pb*-$[Ni(\mathbf{L^2})]^{2+}$) coordination. The stabilization of the octahedral geometry in the Ni^{II} complex can be considered as the result of the Jahn–Teller effect operating in pentagonal-bipyramidal geometry, which in an extreme case leads to an octahedral coordination. Spectrophotometric titrations carried out in dimethyl sulfoxide (DMSO) and CH_3CN/DMSO (9:1) solutions indicate the following stability sequence for the complexes of **L²**: $Co^{II} \approx Ni^{II} > Zn^{II} \gg Mn^{II}$. The variations in the geometry and stability of the complexes may be rationalized in terms of the different occupations of the frontier molecular orbitals along the first-row transition-metal series. Finally, a time-dependent DFT approach was used to investigate the absorption spectrum of the $[Cu(\mathbf{L^2})]^{2+}$ complex based on the optimized geometries at the B3LYP level, also confirming a pentagonal-bipyramidal coordination in solution for this compound.

Introduction

The most commonly observed coordination numbers in first-row transition-metal complexes are four, five, and six, with lower and higher coordination numbers being relatively rare. Even so, two- and three-coordinated complexes of first-row transition-metal complexes have been obtained by using extremely bulky ligands that protect the metal ion from the environment,[1,2] while a few examples of eight-coordinated first-row transition-metal complexes with tetraazamacrocycles have also been reported.[3]

Seven-coordination of first-row transition metals was rarely observed until the 1970s and is still uncommon today. In fact, a recent estimate based on the number of transition-metal σ-bonded complexes found in the Cambridge Structural Database reveals that seven-coordinated complexes only represent 1.8% of the total number of structures reported[4] and that the distribution of seven-coordination throughout the first-row transition-metal series is also quite irregular,

* To whom correspondence should be addressed. E-mail: ucambv@udc.es (A.d.B.), mayter@udc.es (T.R.-B.).

(1) Nguyen, T.; Panda, A.; Olmstead, M. M.; Richards, A. F.; Stender, M.; Brynda, M.; Power, P. P. *J. Am. Chem. Soc.* **2005**, *127*, 8545−8552.

(2) (a) Holland, P. L.; Cundari, T. R.; Perez, L. L.; Eckert, N. A.; Lachicotte, R. J. *J. Am. Chem. Soc.* **2002**, *124*, 14416−14424. (b) Palacios, A. A.; Alemany, J. M.; Álvarez, S. *Inorg. Chem.* **1999**, *38*, 707−715.

(3) (a) Koch, W. O.; Barbieri, A.; Grodzicki, M.; Schünemann, V.; Trautwein, A. X.; Krüger, H.-J. *Angew. Chem., Int. Ed. Engl.* **1996**, *35*, 422−424. (b) Koch, W. O.; Kaiser, J. T.; Krüger, H.-J. *Chem. Commun.* **1997**, 2237−2238.

(4) Casanova, D.; Alemany, P.; Bofia, J. M.; Álvarez, S. *Chem.—Eur. J.* **2003**, *9*, 1281−1295.

10.1021/ic7008946 CCC: $37.00
Published on Web 09/01/2007

being more common for Mn, Fe, and Co[5,6] than for Ni,[7] Cu,[8] or Zn.[9] With seven being an odd coordination number, no regular polyhedron can describe the coordination sphere around a seven-coordinated metal ion. The most commonly observed coordination polyhedra in seven-coordinated transition-metal complexes are pentagonal bipyramid, capped octahedron, and capped trigonal prism,[10] with pentagonal bipyramid being the most common case.[4] However, an unambiguous assignment of the coordination polyhedra in seven-coordinated complexes is sometimes difficult because the same structure resembles more than one reference polyhedra.[4]

The synthesis of first-row transition-metal seven-coordinated complexes required a rational ligand design. Several strategies have been designed for this purpose including the use of acyclic[11] or macrocyclic[13,12] pentadentate ligands, acyclic heptadentate ligands,[5,13] N,N′-disubstituted pentazamacrocycles,[14] or acyclic ligands that stabilize the pentagonal bipyramid by $\pi-\pi$-stacking interactions.[15] The hexadentate ligand ethylenediaminetetraacetate also forms seven-coordinated complexes with several di- and trivalent first-row transition-metal ions,[16] where a water molecule occupies the seventh coordination position of the metal center.

Chart 1

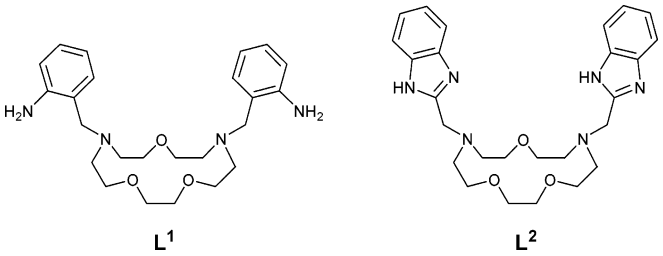

L^1 L^2

In recent works, we have demonstrated that receptor *N*,*N*′-bis(2-aminobenzyl)-1,10-diaza-15-crown-5 ($\mathbf{L^1}$, Chart 1) yields mononuclear divalent first-row transition-metal-ion complexes (M = Mn, Co, Ni, Cu, or Zn) with pentagonal-bipyramidal geometry.[17−19] In these complexes, the oxa-aza crown moiety provides the five donor atoms of the equatorial plane while the donor atoms of the pendant arms occupy the apical coordination positions, and we have demonstrated that the structural features and electronic properties of $[M(\mathbf{L^1})]^{2+}$ complexes (M = Mn, Co, Ni, or Zn) can be rationalized by using density functional theory (DFT) calculations based on the B3LYP model.[18,19]

As a continuation of our previous works in this field, herein we report the synthesis and characterization of new complexes of divalent first-row transition-metal ions with the heptadentate ligand *N*,*N*′-bis(benzimidazol-2-ylmethyl)-1,10-diaza-15-crown-5 ($\mathbf{L^2}$, Chart 1). This receptor contains benzimidazol-2-ylmethyl pendant arms that are expected to form five-membered chelate rings upon coordination to the metal ion, in contrast to the 2-aminobenzyl pendants of $\mathbf{L^1}$, which form six-membered chelate rings. To rationalize the experimental results, we have performed a theoretical study of the $[M(\mathbf{L^2})]^{2+}$ systems (M = Mn, Co, Ni, Cu, or Zn) at the DFT (B3LYP) computational level and a molecular orbital (MO) analysis. Likewise, a time-dependent DFT (TDDFT) approach has been used to investigate the absorption spectra of the $[Cu(\mathbf{L^2})]^{2+}$ complex.

Experimental Section

Chemicals and Starting Materials. *N*,*N*′-Bis(benzimidazol-2-ylmethyl)-1,10-diaza-15-crown-5 ($\mathbf{L^2}$) was prepared as previously reported.[20] All other chemicals were purchased from commercial sources and used without further purification. Solvents were of reagent grade and were purified by the usual methods, unless otherwise stated. ***Caution!*** *Although we have experienced no difficulties with the perchlorate salts, these should be regarded as potentially explosive and handled with care.*[21]

Physical Methods. Elemental analyses were carried out on a Carlo Erba 1108 elemental analyzer. Fast atom bombardment mass spectrometry (FAB-MS) spectra were recorded using a FISONS

(5) (a) Gou, S.; You, X.; Yu, K.; Lu, J. *Inorg. Chem.* **1993**, *32*, 1883−1887. (b) Horner, O.; Girerd, J.-J.; Philouze, C.; Tchertanov, L. *Inorg. Chim. Acta* **1999**, *290*, 139−144.

(6) (a) Baffert, C.; Romero, I.; Pecaut, J.; Llobet, A.; Deronzier, A.; Collomb, M.-N. *Inorg. Chim. Acta* **2004**, *357*, 3430−3436. (b) Capparelli, M. V.; De Meester, P.; Goodgame, D. M. L.; Gunn, S. J.; Skapski, A. C. *Inorg. Chim. Acta* **1985**, *97*, L37−L39.

(7) (a) Wester, D.; Palenik, G. J. *J. Am. Chem. Soc.* **1974**, *96*, 7565−7566. (b) Giordano, T. J.; Palenik, G. J.; Palenik, R. C.; Sullivan, D. A. *Inorg. Chem.* **1979**, *18*, 2445−2450.

(8) (a) Melník, M.; Kabesová, M.; Makásková, L.; Holloway, C. E. *J. Coord. Chem.* **1998**, *45*, 31−145. (b) Marquez, V. E.; Anacona, J. R.; Loroño, D. *Polyhedron* **2004**, *23*, 1317−1323.

(9) Adam, K. R.; Donnelly, S.; Leong, A. J.; Lindoy, L. F.; McCool, B. J.; Bashall, A.; Dent, M. R.; Murphy, B. P.; McPartlin, M.; Fenton, D. E.; Tasker, P. A. *J. Chem. Soc., Dalton Trans.* **1990**, 1635−1643.

(10) Hoffmann, R.; Beier, B. F.; Muetterties, E. L.; Rossi, A. R. *Inorg. Chem.* **1977**, *16*, 511−522.

(11) Ivanovic-Burmazovic, I.; Andjelkovic, K. *Adv. Inorg. Chem.* **2004**, *55*, 315−360.

(12) (a) Drew, M. G. B.; bin Toman, A. H.; McFall, S. G.; McIlroy, P. D. A.; Nelson, S. M. *J. Chem. Soc., Dalton Trans*. **1977**, 1173−1180. (b) Bencini, A.; Bianchi, A.; Dapporto, P.; Garcia-Espana, E.; Marcelino, V.; Micheloni, M.; Paoletti, P.; Paoli, P. *Inorg. Chem*. **1990**, *29*, 1716−1718. (c) Marquez, V. E.; Anacona, J. R.; Rodriguez Barbarin, C. *Polyhedron* **2001**, *20*, 1885−1890. (d) Gerloch, M.; Hanton, L. R. *Inorg. Chim. Acta* **1981**, *49*, 37−45.

(13) Kirchner, R. M.; Mealli, C.; Bailey, M.; Howe, N.; Torre, L. P.; Wilson, L. J.; Andrews, L. C.; Rose, N. J.; Lingafelter, E. C. *Coord. Chem. Rev.* **1987**, *77*, 89−163. Yang, S.-P.; Tong, Y.-X.; Zhu, H.-L.; Cao, H.; Chen, X.-M.; Ji, L.-N. *Polyhedron* **2001**, *20*, 223−229. Salehzadeh, S.; Javarsineh, S. A.; Keypour, H. *J. Mol. Struct.* **2006**, *785*, 54−62.

(14) Park, W.; Shin, M. H.; Chung, J. H.; Park, J.; Lah, M. S.; Lim, D. *Tetrahedron Lett.* **2006**, *47*, 8841−8845.

(15) Seitz, M.; Kaiser, A.; Stempfhuber, S.; Zabel, M.; Reiser, O. *Inorg. Chem.* **2005**, *44*, 4630−4636.

(16) (a) Lopez-Alcala, J. M.; Puerta-Vizcaino, M. C.; Gonzalez-Vilchez, F.; Duesler, E. N.; Tapscott, R. E. *Acta Crystallogr., Sect. C* **1984**, *C40*, 939−941. (b) Shimoi, M.; Saito, Y.; Ogino, H. *Bull. Chem. Soc. Jpn.* **1991**, *64*, 2629−2634. (c) Mizuta, T.; Wang, J.; Miyoshi, K. *Inorg. Chim. Acta* **1993**, *203*, 249−252. (d) Mizuta, T.; Wang, J.; Miyoshi, K. *Bull. Chem. Soc. Jpn.* **1993**, *66*, 3662−3670. (e) Mizuta, T.; Wang, J.; Miyoshi, K. *Bull. Chem. Soc. Jpn.* **1993**, *66*, 2547−2551. (f) Zubkowski, J. D.; Perry, D. L.; Valente, E. J.; Lott, S. *Inorg. Chem.* **1995**, *34*, 6409−6411. (g) Richards, S.; Pedersen, B.; Silverton, J. V.; Hoard, J. L. *Inorg. Chem.* **1964**, *3*, 27−33.

(17) Rodríguez-Infante, C.; Esteban, D.; Avecilla, F.; de Blas, A.; Rodríguez-Blas, T.; Mahía, J.; Macedo, A. L.; Geraldes, C. F. G. C. *Inorg. Chim. Acta* **2001**, *317*, 190−198.

(18) Platas-Iglesias, C.; Vaiana, L.; Esteban-Gómez, D.; Avecilla, F.; Real, J. A.; de Blas, A.; Rodríguez-Blas, T. *Inorg. Chem.* **2005**, *44*, 9704−9713.

(19) Vaiana, L.; Platas-Iglesias, C.; Esteban-Gómez, D.; Avecilla, F.; de Blas, A.; Rodríguez-Blas, T. *Eur. J. Inorg. Chem.* **2007**, 1874−1883.

(20) Regueiro-Figueroa, M.; Esteban-Gómez, D.; Platas-Iglesias, C.; de Blas, A.; Rodríguez-Blas, T. *Eur. J. Inorg. Chem.* **2007**, 2198−2207.

(21) Wolsey, W. C. *J. Chem. Educ.* **1973**, *50*, A335−A337.

QUATRO mass spectrometer with a Cs ion gun and 3-nitrobenzyl alcohol as the matrix. IR spectra were recorded, as KBr disks, using a Bruker Vector 22 spectrophotometer. Conductivity measurements were carried out at 20 °C with a Crison Micro CM 2201 conductimeter using 10^{-3} M solutions of the complexes in acetonitrile. Variable-temperature magnetic susceptibility measurements were carried out using microcrystalline samples (20−60 mg) of the Mn, Co, Ni, and Cu compounds using a Quantum Design Physical Property Measurement System operating at 0.5 T and at temperatures from 79 to 300 K for Mn, Ni, and Cu compounds and from 300 to 2 K for the Co one. Experimental susceptibilities were corrected for diamagnetism of the constituent atoms by the use of Pascal's constants. ^{1}H and ^{13}C NMR spectra were run on a Bruker Avance 500 MHz spectrometer. Chemical shifts are reported in parts per million with respect to tetramethylsilane (TMS). Spectral assignments were based on two-dimensional COSY, HSQC, and HMBC experiments. UV−vis spectra were recorded on a Perkin-Elmer Lambda 900 spectrophotometer, with quartz cells (path length: 1 cm). The cell holder was thermostated at 25 °C, through circulating water. The formation of the $[M(\mathbf{L^2})]^{2+}$ complexes (M = Mn, Co, Ni, Cu, or Zn) was monitored by means of spectrophotometric titrations at 25 °C on 10^{-4} M solutions of $\mathbf{L^2}$ in dimethyl sulfoxide (DMSO) or CH_3CN/DMSO (9:1, v/v) mixtures (polarographic grade). Typically, aliquots of a fresh 10^{-2} M standard solution of the envisaged perchlorate salt in the same solvent were added, and the UV−vis spectra of the samples were recorded. The formation of the $[M(\mathbf{L^2})]^{2+}$ complexes (M = Mn, Co, or Ni) was also followed by competitive titration experiments in CH_3CN/DMSO (9:1, v/v) mixtures. In the case of the Co^{II} and Ni^{II} complexes, a 10^{-4} M solution of $\mathbf{L^2}$ was titrated with a fresh standard 0.1 M solution of the corresponding perchlorate salt in the presence of 1 equiv of zinc(II) perchlorate, while for the Mn^{II} complex, a 10^{-4} M solution of $\mathbf{L^2}$ was titrated with a fresh standard 0.1 M solution of zinc(II) perchlorate in the presence of 1 equiv of Mn^{II}. All spectrophotometric titration curves were fitted with the *HYPERQUAD* program.[22]

Synthesis of the Complexes. $[Mn(\mathbf{L^2})](ClO_4)_2\cdot H_2O$ ($\mathbf{MnL^2}$). A mixture of $\mathbf{L^2}$ (0.080 g, 0.167 mmol) and $Mn(ClO_4)_2\cdot 6H_2O$ (0.061 g, 0.169 mmol) in 2-propanol (35 mL) was stirred and heated to reflux over a period of 6 h. The brown precipitate formed was isolated by filtration and air-dried (yield: 0.104 g, 83%). Anal. Calcd for $C_{26}H_{34}Cl_2MnN_6O_{11}\cdot H_2O$: C, 41.61; H, 4.84; N, 11.20. Found: C, 41.58; H, 4.67; N, 11.04. Λ_M (acetonitrile): 285 $cm^2\ \Omega^{-1}\ mol^{-1}$ (2:1 electrolyte). IR (KBr): 1621 [ν(C═N)], 1540 [ν(C═C)], 1091 [ν_a(Cl−O)], 626 [δ_a(O−Cl−O)] cm^{-1}. FAB-MS (*m/z* (% BPI)): 632 (34) $[Mn(\mathbf{L^2})(ClO_4)]^+$, 532 (100) $[Mn(\mathbf{L^2}-H)]^+$.

$[Co(\mathbf{L^2})](ClO_4)_2$ ($\mathbf{CoL^2}$). The preparation of the brown complex followed the same procedure as that described for $\mathbf{MnL^2}$ by using $\mathbf{L^2}$ (0.100 g, 0.209 mmol) and $Co(ClO_4)_2\cdot 6H_2O$ (0.077 g, 0.210 mmol) in 30 mL of 2-propanol (yield: 0.119 g, 77%). Anal. Calcd for $C_{26}H_{34}Cl_2CoN_6O_{11}$: C, 42.40; H, 4.65; N, 11.41. Found: C, 42.68; H, 4.92; N, 11.35. Λ_M (acetonitrile): 276 $cm^2\ \Omega^{-1}\ mol^{-1}$ (2:1 electrolyte). IR (KBr): 1623 [ν(C═N)], 1543 [ν(C═C)], 1091 [ν_a(Cl−O)], 626 [δ_a(O−Cl−O)] cm^{-1}. FAB-MS (*m/z* (% BPI)): 636 (29) $[Co(\mathbf{L^2})(ClO_4)]^+$, 536 (100) $[Co(\mathbf{L^2}-H)]^+$.

$[Ni(\mathbf{L^2})](ClO_4)_2$ ($\mathbf{NiL^2}$). The preparation of the green complex followed the same procedure as that described for $\mathbf{MnL^2}$ by using $\mathbf{L^2}$ (0.101 g, 0.211 mmol) and $Ni(ClO_4)_2\cdot 6H_2O$ (0.077 g, 0.210 mmol) in 35 mL of 2-propanol (yield: 0.117 g, 75%). Anal. Calcd for $C_{26}H_{34}Cl_2NiN_6O_{11}$: C, 42.42; H, 4.66; N, 11.42. Found: C, 42.35; H, 5.00; N, 11.52. Λ_M (acetonitrile): 265 $cm^2\ \Omega^{-1}\ mol^{-1}$ (2:1 electrolyte). IR (KBr): 1622 [ν(C═N)], 1546 [ν(C═C)], 1087 [ν_a(Cl−O)], 627 [δ_a(O−Cl−O)] cm^{-1}. FAB-MS (*m/z* (% BPI)): 635 (10) $[Ni(\mathbf{L^2})(ClO_4)]^+$, 535 (100) $[Ni(\mathbf{L^2}-H)]^+$. Single crystals of formula $[Ni(\mathbf{L^2})](ClO_4)_2\cdot H_2O$ were obtained by slow diffusion of diethyl ether into a solution of the complex in acetonitrile.

$[Cu(\mathbf{L^2})](ClO_4)_2\cdot H_2O$ ($\mathbf{CuL^2}$). The preparation of the green complex followed the same procedure as that described for $\mathbf{MnL^2}$ by using $\mathbf{L^2}$ (0.100 g, 0.209 mmol) and $Cu(ClO_4)_2\cdot 6H_2O$ (0.078 g, 0.211 mmol) in 30 mL of 2-propanol (yield: 0.138 g, 85%). Anal. Calcd for $C_{26}H_{34}Cl_2CuN_6O_{11}\cdot H_2O$: C, 41.14; H, 4.78; N, 11.07. Found: C, 41.29; H, 5.05; N, 10.81. Λ_M (acetonitrile): 250 $cm^2\ \Omega^{-1}\ mol^{-1}$ (2:1 electrolyte). IR (KBr): 1622 [ν(C═N)], 1550 [ν(C═C)], 1090 [ν_a(Cl−O)], 626 [δ_a(O−Cl−O)] cm^{-1}. FAB-MS (*m/z* (% BPI)): 641 (18) $[Cu(\mathbf{L^2})(ClO_4)]^+$, 541 (100) $[Cu(\mathbf{L^2}-H)]^+$.

$[Zn(\mathbf{L^2})](ClO_4)_2$ ($\mathbf{ZnL^2}$). A mixture of $\mathbf{L^2}$ (0.100 g, 0.209 mmol) and $Zn(ClO_4)_2\cdot 6H_2O$ (0.078 g, 0.210 mmol) in ethanol (50 mL) was stirred and heated to reflux over a period of 4 h, and the yellow solution was filtered while hot. Slow diffusion of diethyl ether into the former solution at room temperature gave colorless single crystals that were isolated by filtration and air-dried (yield: 0.101 g, 65%). Anal. Calcd for $C_{26}H_{34}Cl_2N_6O_{11}Zn$: C, 42.04; H, 4.61; N, 11.31. Found: C, 41.97; H, 4.97; N, 11.36. Λ_M (acetonitrile): 288 $cm^2\ \Omega^{-1}\ mol^{-1}$ (2:1 electrolyte). IR (KBr): 1622 [ν(C═N)], 1544 [ν(C═C)], 1086 [ν_a(Cl−O)], 626 [δ_a(O−Cl−O)] cm^{-1}. FAB-MS (*m/z* (% BPI)): 641 (15) $[Zn(\mathbf{L^2})(ClO_4)]^+$, 541 (100) $[Zn(\mathbf{L^2}-H)]^+$.

Crystal Structure Determination. Three-dimensional X-ray data were collected at 100 K on a Bruker X8-APEXII Kappa diffractometer by the Ω/ϕ-scan method ($\mathbf{NiL^2}$) or on a Bruker SMART 1000 CCD diffractometer by the Ω-scan method ($\mathbf{ZnL^2}$). Reflections were measured from a hemisphere of data collected of frames each covering 0.3° in Ω. The solution, refinement, and analysis of the single-crystal X-ray diffraction data was performed with the *WinGX* suite for small-molecule single-crystal crystallography.[23] The structures were solved by Patterson methods with *DIRDIF99*[24] and refined by full-matrix least-squares methods on F^2 with *SHELX97*.[25] The H atoms were included in calculated positions and refined by using a riding mode, except H atoms of the water molecule in $\mathbf{NiL^2}$ compound, which were found in a Fourier difference map, and all of the positional parameters were fixed. Refinement converged with allowance for thermal anisotropy of all non-H atoms. Crystal data and details on data collection and refinement are summarized in Table 1.

DFT Studies. The $[M(\mathbf{L^2})]^{2+}$ (M = Mn, Co, Ni, or Cu) systems were fully optimized in vacuo by using the UB3LYP DFT model.[26] On the grounds of our previous experience,[18,19] in these calculations we used a mixed basis set, comprising the standard 6-31G(d) basis on N, C, H, and O atoms and Ahlrichs' valence triple-ζ (VTC) on the metal atoms.[27] All complexes were modeled in their high-spin configurations (Mn, $S = {}^5/_2$; Co, $S = {}^3/_2$; Ni, $S = 1$; Cu, $S = {}^1/_2$), and wavefunction stability calculations were performed (using the

(22) Gans, P.; Sabatini, A.; Vacca, A. *Talanta* **1996**, *43*, 1739−1753.

(23) *WinGX* 1.70.01: an integrated system of Windows programs for the solution, refinement, and analysis of single-crystal X-ray diffraction data. Farrugia, L. J. *J. Appl. Crystallogr.* **1999**, *32*, 837−838.

(24) Beurskens, P. T.; Beurskens, G.; de Gelder, R.; Garcia-Granda, S.; Gould, R. O.; Israel, R.; Smits, J. M. M. *DIRDIF99 program system*; Crystallography Laboratory, University of Nijmegen: Nijmegen, The Netherlands, 1999.

(25) Sheldrick, G. M. *SHELX97*: *Programs for Crystal Structure Analysis*, release 97-2; Institüt für Anorganische Chemie der Universität: Göttingen, Germany, 1998.

(26) (a) Becke, A. D. *J. Chem. Phys.* **1993**, *98*, 5648−5652. (b) Lee, C.; Yang, W.; Parr, R. G. *Phys. Rev. B* **1988**, *37*, 785−789.

(27) Schäefer, A.; Horn, H.; Ahlrichs, R. *J. Chem. Phys.* **1992**, *97*, 2571−2577.

Table 1. Crystal Data and Structure Refinement for $\mathbf{NiL^2}$ and $\mathbf{ZnL^2}$

formula	$C_{26}H_{36}Cl_2N_6NiO_{12}$	$C_{26}H_{34}Cl_2N_6O_{11}Zn$
mol wt	754.22	742.86
temp/K	100.0(1)	100(2)
cryst syst	monoclinic	triclinic
space group	$P2_1/n$	$P\bar{1}$
a/Å	11.4318(3)	11.050(3)
b/Å	17.0988(4)	12.046(3)
c/Å	15.6524(4)	13.570(4)
α/deg	90	94.609(6)
β/deg	92.266(2)	109.246(5)
γ/deg	90	112.763(5)
V/Å^3	3057.2(1)	1527.0(7)
Z	4	2
λ(Mo Kα)/Å	0.710 73	0.710 73
D_{calc}/g cm^{-3}	1.639	1.616
μ/mm^{-1}	0.884	1.049
F(000)	1568	768
R_{int}	0.1047	0.1087
reflns collected	30 237	15 721
indep reflns	6285	5817
reflns gt	3825	2960
GOF on F^2	1.065	1.008
final R indices $[I > 2\sigma(I)]^a$	R1 = 0.0707, wR2 = 0.1581	R1 = 0.0603, wR2 = 0.1242
R indices (all data)^a	R1 = 0.1245, wR2 = 0.1784	R1 = 0.1536, wR2 = 0.1611
largest diff peak and hole/e Å^{-3}	1.85 and −1.378	1.133 and −1.041

^{a} $R1 = \sum||F_o| - |F_c||/\sum|F_o|$. $wR2 = \{\sum[w(|F_o|^2 - |F_c|^2)^2]/\sum[w(F_o^4)]\}^{1/2}$.

stable keyword in *Gaussian 03*) to confirm that the calculated wavefunction corresponded to the ground state. Because geometry optimizations were performed by using an unrestricted model, spin contamination[28] was assessed by a comparison of the expected difference between $S(S + 1)$ for the assigned spin state and the actual value of $\langle S^2 \rangle$.[29] The results (Table S1 in the Supporting Information) indicate that spin contamination is negligible for every $[M(\mathbf{L^2})]^{2+}$ system. Full geometry optimizations of the $[Zn(\mathbf{L^2})]^{2+}$ system were performed at the RB3LYP level by using the same combination of basis sets described above. For the $[Ni(\mathbf{L^2})]^{2+}$ system, two different conformations giving rise to octahedral (*o*-$[Ni(\mathbf{L^2})]^{2+}$) and pentagonal-bipyramidal (*pb*-$[Ni(\mathbf{L^2})]^{2+}$) coordination geometries were calculated. The stationary points found on the potential energy surfaces as a result of the geometry optimizations have been tested to represent energy minima rather than saddle points via frequency analysis.

The NMR shielding tensors of the $[Zn(\mathbf{L^2})]^{2+}$ system were calculated both in vacuo and in an acetonitrile solution by using the GIAO method.[30] In these calculations, we have used the 6-311G-(d,p) basis set on ligand atoms and Ahlrichs' VTC for Zn. For ^{13}C NMR chemical shift calculation purposes, the NMR shielding tensors of TMS were calculated at the appropriate level. Solvent effects were evaluated by using the polarizable continuum model (PCM). In particular, we selected the C-PCM[31] variant that, employing conductor rather than dielectric boundary conditions, allows a more robust implementation. In line with the united atom topological model,[32] the solute cavity is built as an envelope of spheres centered on atoms or atomic groups with appropriate radii.

TDDFT[33] calculations were used for the calculation of the 10 lowest-energy electronic transitions of the $[Cu(\mathbf{L^2})]^{2+}$ complex in the gas phase. All calculations were performed by using the *Gaussian 03* package (revision C.01).[34] Overlap population density-of-states (ODOS) values were obtained by using the *PyMOlyze* program.[35]

Results

Synthesis and Characterization of the Complexes. Reaction of $\mathbf{L^2}$ with the appropriate hydrated perchlorate salt led to compounds of formula $[M(\mathbf{L^2})](ClO_4)_2$ (M = Mn, Co, Ni, Cu, or Zn) in good yield (65−85%). In the following, these compounds will be denoted as $\mathbf{ML^2}$ (**M = Mn**, **Co**, **Ni**, **Cu**, or **Zn**). The IR spectra (KBr disks) show a band at ca. 1540 cm^{-1} due to the ν(C═C) stretching frequency of the benzimidazole group. This band is shifted by 10−15 cm^{-1} to higher wavenumbers with respect to its position in the spectra of the free ligand. Bands corresponding to the ν_{as}(Cl−O) stretching and δ_{as}(O−Cl−O) bending modes of the ionic perchlorate groups appear at ca. 1086 and 626 cm^{-1}, respectively.[36] The FAB-MS spectra of these complexes display an intense peak (100% BPI) due to $[M(\mathbf{L^2}-H)]^+$, which confirms the formation of the complexes. The molar conductivity values, as measured in 10^{-3} M acetonitrile solutions of the complexes, fall in the range generally accepted for 2:1 electrolytes in this solvent (220−300 cm^2 Ω^{-1} mol^{-1}),[37] suggesting that the perchlorate anions are not coordinated to the metal ion in solution.

The $\chi_M T$ products (where χ_M is the molar magnetic susceptibility and T the temperature) measured for Mn, Ni, and Cu compounds remain practically constant in the range of temperatures 79−300 K (Figure S1 in the Supporting Information), with $\chi_M T$ values in agreement with $S = {}^3/_2$ (Mn), $S = 1$ (Ni), and $S = {}^1/_2$ (Cu) ground states, respectively. For the Co compound, the $\chi_M T$ product at 300 K (2.28 cm^3 K mol^{-1}) is larger than that expected for the spin-only formula for a mononuclear high-spin Co^{II} complex

(28) Stanton, J. F.; Gauss, J. *Adv. Chem. Phys.* **2003**, *125*, 101−146.
(29) Montoya, A.; Truong, T. N.; Sarofim, A. F. *J. Phys. Chem. A* **2000**, *124*, 6108−6110.
(30) Ditchfield, R. *Mol. Phys.* **1974**, *27*, 789−807.
(31) (a) Barone, V.; Cossi, M. *J. Phys. Chem. A* **1998**, *102*, 1995−2001. (b) Cossi, M.; Rega, N.; Scalmani, G.; Barone, V. *J. Comput. Chem.* **2003**, *24*, 669−681.
(32) Barone, V.; Cossi, M.; Tomasi, J. *J. Chem. Phys.* **1997**, *107*, 3210−3221.
(33) (a) Stratmann, R. E.; Scuseria, G. E.; Frisch, M. J. *J. Chem. Phys.* **1998**, *109*, 8218−8224. (b) Bauernschmitt, R.; Ahlrichs, R. *Chem. Phys. Lett.* **1996**, *256*, 454−464. (c) Casida, M. E.; Jamorski, C.; Casida, K. C.; Salahub, D. R. *J. Chem. Phys.* **1998**, *108*, 4439−4449.
(34) Frisch, M. J.; Trucks, G. W.; Schlegel, H. B.; Scuseria, G. E.; Robb, M. A.; Cheeseman, J. R.; Montgomery, J. A., Jr.; Vreven, T.; Kudin, K. N.; Burant, J. C.; Millam, J. M.; Iyengar, S. S.; Tomasi, J.; Barone, V.; Mennucci, B.; Cossi, M.; Scalmani, G.; Rega, N.; Petersson, G. A.; Nakatsuji, H.; Hada, M.; Ehara, M.; Toyota, K.; Fukuda, R.; Hasegawa, J.; Ishida, M.; Nakajima, T.; Honda, Y.; Kitao, O.; Nakai, H.; Klene, M.; Li, X.; Knox, J. E.; Hratchian, H. P.; Cross, J. B.; Adamo, C.; Jaramillo, J.; Gomperts, R.; Stratmann, R. E.; Yazyev, O.; Austin, A. J.; Cammi, R.; Pomelli, C.; Ochterski, J. W.; Ayala, P. Y.; Morokuma, K.; Voth, G. A.; Salvador, P.; Dannenberg, J. J.; Zakrzewski, V. G.; Dapprich, S.; Daniels, A. D.; Strain, M. C.; Farkas, O.; Malick, D. K.; Rabuck, A. D.; Raghavachari, K.; Foresman, J. B.; Ortiz, J. V.; Cui, Q.; Baboul, A. G.; Clifford, S.; Cioslowski, J.; Stefanov, B. B.; Liu, G.; Liashenko, A.; Piskorz, P.; Komaromi, I.; Martin, R. L.; Fox, D. J.; Keith, T.; Al-Laham, M. A.; Peng, C. Y.; Nanayakkara, A.; Challacombe, M.; Gill, P. M. W.; Johnson, B.; Chen, W.; Wong, M. W.; Gonzalez, C.; Pople, J. A. *Gaussian 03*; Gaussian, Inc.: Wallingford, CT, 2004.
(35) Tenderholt, A. L. *PyMOlyze: A Program to Analyze Quantum Chemistry Calculations*, version 2.0, http://pymolyze.sourceforge.net.
(36) Nakamoto, K. *Infrared and Raman Spectra of Inorganic and Coordination Compounds*, 5th ed.; John Wiley & Sons, Inc.: New York, 1997.
(37) Geary, W. J. *Coord. Chem. Rev.* **1971**, *7*, 81−122.

Table 2. Experimental and Calculated Bond Lengths (Å) and Angles (deg) of the Metal Coordination Environment in *bp*-[M(**L²**)]$^{2+}$ Complexes (M = Mn, Co, Ni, Cu, or Zn)

					[Zn(**L²**)]$^{2+}$	
	[Mn(**L²**)]$^{2+}$ [a]	[Co(**L²**)]$^{2+}$ [a]	[Ni(**L²**)]$^{2+}$ [a]	[Cu(**L²**)]$^{2+}$ [a]	calcd[a]	exp[b]
M1−O2	2.275	2.243	2.111	2.267	2.248	2.273(4)
M1−O1	2.275	2.227	2.110	2.267	2.248	2.284(4)
M1−O3	2.281	2.306	2.571	2.382	2.315	2.257(4)
M1−N2	2.243	2.141	2.075	2.024	2.103	2.117(5)
M1−N6	2.243	2.128	2.075	2.024	2.103	2.109(5)
M1−N3	2.415	2.337	2.354	2.355	2.355	2.256(5)
M1−N4	2.415	2.243	2.360	2.355	2.355	2.260(5)
N6−M1−N2	176.18	178.27	177.83	179.11	177.13	168.7(2)
N6−M1−N3	106.36	103.91	100.46	101.47	102.85	104.0(2)
N2−M1−N3	75.01	77.49	78.56	78.87	78.21	79.5(2)
N6−M1−O3	91.91	89.90	88.82	90.44	91.44	94.2(2)
N2−M1−O3	91.91	91.56	89.01	90.44	91.44	97.1(2)
N3−M1−O3	69.96	69.13	63.69	67.90	68.84	69.7(2)
N6−M1−N4	75.02	77.48	78.45	78.87	78.21	80.3(2)
N2−M1−N4	106.34	102.20	100.58	101.47	102.85	104.4(2)
N3−M1−N4	139.87	137.77	127.28	135.81	137.67	139.0(2)
O3−M1−N4	69.92	68.66	63.59	67.90	68.83	69.3(2)
N6−M1−O2	87.53	89.58	90.42	89.71	88.49	86.1(2)
N2−M1−O2	89.40	90.01	91.26	89.58	89.20	85.2(2)
N3−M1−O2	144.66	146.26	154.13	147.56	146.34	144.6(2)
O3−M1−O2	143.41	142.81	140.64	143.14	143.41	144.4(2)
N4−M1−O2	74.65	74.95	77.73	75.99	75.37	75.8(2)
N6−M1−O1	89.38	89.36	91.33	89.58	89.21	85.0(2)
N2−M1−O1	87.56	90.01	90.35	89.71	88.49	85.5(2)
N3−M1−O1	74.65	75.79	77.91	75.99	75.38	75.5(2)
O3−M1−O1	143.43	143.62	140.92	143.14	143.41	143.9(2)
N4−M1−O1	144.66	145.85	153.93	147.56	146.33	145.0(2)
O2−M1−O1	73.16	73.57	78.44	73.73	73.17	71.6(2)

[a] From B3LYP-optimized geometries. [b] From X-ray diffraction analyses.

($S = {}^3/_2$), indicating that a relevant orbital contribution is involved. $\chi_M T$ remains constant from room temperature down to 90 K and then decreases significantly when cooling, reaching a value of 1.15 cm^3 K mol^{-1} at 2.0 K. This magnetic behavior may be associated with the occurrence of zero-field splitting of the orbitally nondegenerate $S = {}^3/_2$ ground state of Co^{II}. The analysis of the magnetic data provides the following parameters that best match the experimental data: $D = 23.1$ cm^{-1}, $g_{x,y} = 2.21$, and $\theta = -0.49$, with $R = 4.4 \times 10^{-4}$. R is the agreement factor defined as $\sum_i[(\chi_M)_i^{exptl}] - [(\chi_M)_i^{calc}]^2/[(\chi_M)_i^{exptl}]^2$. The crystal-field parameter obtained is very similar to that reported for the corresponding complex of **L¹** ($D = 25$ cm^{-1}).[18]

The solid-state structures of the Ni and Zn compounds were determined by single-crystal X-ray diffraction analyses. Crystals contain the cations [M(**L²**)]$^{2+}$ (M = Ni or Zn) and two perchlorate anions that are hydrogen-bonded to the NH groups of the benzimidazole units. Tables 2 and 3 summarize selected bond lengths and angles of the metal coordination environments, while the structures of the [M(**L²**)]$^{2+}$ cations are depicted in Figure 1. Both cation complexes show a slightly distorted C_2 symmetry, with the receptor **L²** arranged in an anti conformation, with both pendant arms pointing to opposite sides of the crown moiety. In both cases, the corresponding metal ion is placed in the macrocyclic cavity, with the donor atoms of the pendant arms apically coordinated. However, the different nature of the guest metal ion results in a different coordination environment around the metal ion; that in the cation [Zn(**L²**)]$^{2+}$ can be described as a distorted pentagonal bipyramid, whereas that in [Ni(**L²**)]$^{2+}$ is best described as a distorted octahedron.

Table 3. Experimental and Calculated Bond Lengths (Å) and Angles (deg) of the Metal Coordination Environment in *o*-[Ni(**L²**)]$^{2+}$

	calcd[a]	exp[b]		calcd[a]	exp[b]
Ni1−O2	2.092	2.069(3)	Ni1−N6	2.084	2.067(4)
Ni1−O1	2.098	2.094(3)	Ni1−N3	2.255	2.195(5)
Ni1−N2	2.074	2.077(4)	Ni1−N4	2.287	2.196(4)
N6−Ni1−O2	90.56	93.1(2)	N2−Ni1−N3	80.44	81.3(2)
N6−Ni1−N2	177.75	179.4(2)	O1−Ni1−N3	80.83	81.1(2)
O2−Ni1−N2	89.70	86.6(2)	N6−Ni1−N4	78.93	80.7(2)
N6−Ni1−O1	91.22	89.2(2)	O2−Ni1−N4	80.86	81.6(2)
O2−Ni1−O1	78.39	78.2(1)	N2−Ni1−N4	98.91	98.7(2)
N2−Ni1−O1	91.02	91.3(2)	O1−Ni1−N4	156.91	156.9(2)
N6−Ni1−N3	100.12	99.2(2)	N3−Ni1−N4	121.24	120.9(2)
O2−Ni1−N3	156.79	155.7(2)			

[a] From B3LYP-optimized geometries. [b] From X-ray diffraction analyses.

The cation [Zn(**L²**)]$^{2+}$ contains a ZnN_4O_3 core with the seven heteroatoms of **L²** coordinated to the metal ion. The equatorial plane of the pentagonal bipyramid is defined by the three ether O atoms and the two pivotal N atoms (mean deviation from planarity: 0.134 Å). The polyhedron is axially compressed because the apical bonds are significantly shorter than the equatorial bonds. Angle N2−Zn1−N6 [168.7(2)°] deviates by ca. 11° from the ideal value for a regular pentagonal bipyramid (180°). Angles D1−Zn1−D2, where D1 and D2 represent adjacent donor atoms of the equatorial plane, are close to the ideal value of 72° (Table 2), and the vectors defined by the metal ion and the axial donors N2 and N6 form angles that are relatively close to 90°, with

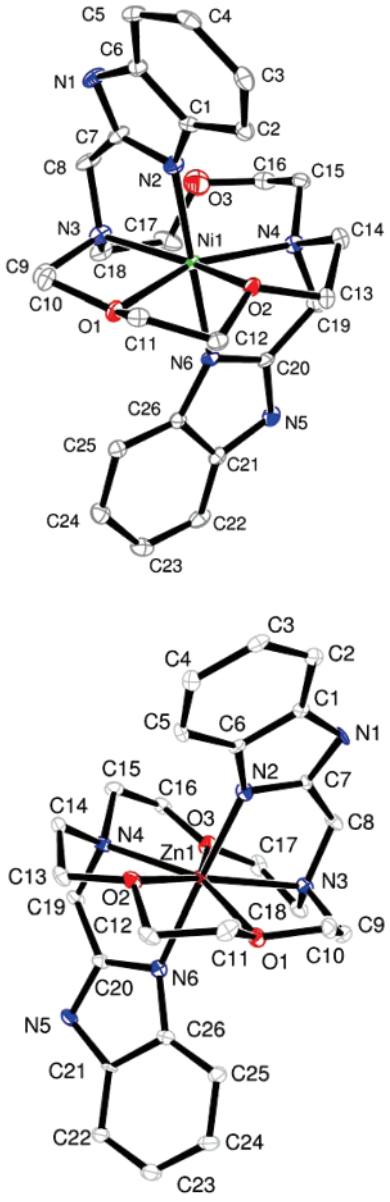

Figure 1. X-ray crystal structure of the cations $[M(\mathbf{L^2})]^{2+}$ in $\mathbf{NiL^2}$ (top) and $\mathbf{ZnL^2}$ (bottom) with atom labeling. H atoms are omitted for simplicity. The ORTEP plots are drawn at the 30% probability level.

the vectors containing the metal ion and the equatorial donor atoms, as expected for a pentagonal-bipyramidal coordination environment. On the other hand, in $[Ni(\mathbf{L^2})]^{2+}$, the distance between the Ni^{II} ion and the third O atom of the crown moiety is too long to be considered as a bond distance [Ni1−O3 = 3.330(5) Å], and only six of the seven available donors belong to the Ni^{II} coordination sphere. One of the equatorial planes of the octahedron is defined by the two ether O atoms (O1 and O2) and the two pivotal N atoms (mean deviation from planarity: 0.151 Å). The trans angle N2−Ni1−N6 [179.4(2)°] is relatively close to the expected value for a regular octahedron (180°). Three of the cis angles of the equatorial plane are considerably smaller than the ideal value of 90°, while the fourth cis angle of the equatorial plane is considerably larger [N3−Ni1−N4 = 120.93(17)°], as expected for an eight-membered chelate ring.[38] In any case, the vectors defined by the metal ion and the axial donors N2 and N6 form angles relatively close to 90°, with the vectors containing the metal ion and the equatorial donor atoms, as expected for an octahedral coordination environment. The Ni1−N2 and Ni1−N6 distances are close to those observed in other Ni^{II} six-coordinated complexes with ligands containing benzimidazole groups,[39] and the distances between the metal ion and the donor atoms of the crown moiety (Table 3) are also within the normal range observed in related systems.[19,40]

The ^1H and ^{13}C NMR spectra of the Zn compound were recorded in a CD_3CN solution and partially assigned on the basis of two-dimensional COSY, HSQC, and HMBC experiments (Figure 2). The ^{13}C NMR spectrum (Table 4) shows 13 signals for the 26 C nuclei of the ligand backbone, pointing to an effective C_2 symmetry of the complex in solution. Significant changes in the chemical shifts and the structure of the signals are observed in the ^1H NMR spectra upon coordination of the ligand [20] to the Zn^{II} ion (Figure 2). The most complicated region of the spectra is that where the ethylene and methylene proton signals are observed. Because assignments to specific axial/equatorial CH_2 protons were not possible on the basis of the two-dimensional NMR spectra, they were carried out using the stereochemically dependent proton shift effects, resulting from the polarization of the C−H bonds by the electric field generated by the cation charge,[41] as predicted from the calculated structure of $[Zn(\mathbf{L^2})]^{2+}$. This polarization results in a deshielding of the equatorial protons, which are pointing away from the metal ion (Figure 2). The H8 methylene protons show an AB pattern ($^2J_{8a-8b}$ = 18.8 Hz), in which the protons labeled as b are again deshielded because they are pointing away the metal ion. Furthermore, a specific assignment of several pairs of NMR signals (2−5, 3−4, 9−11, and 10−12) was not possible on the basis of the two-dimensional spectra. To aid the experimental assignments, the ^{13}C NMR shielding constants of $[Zn(\mathbf{L^2})]^{2+}$ were calculated on the DFT-optimized structure of $[Zn(\mathbf{L^2})]^{2+}$ (vide infra) by using the GIAO method. This method has been shown to provide theoretical ^{13}C NMR shifts in good agreement with the

(38) (a) Jurison, S.; Aston, K.; Fair, C. K.; Schlemper, E. O.; Sharp, P. R.; Troutner, D. E. *Inorg. Chem.* **1987**, *26*, 3576−3582. (b) Amoedo-Portela, A.; Carballo, R.; Casas, J. S.; Garcia-Martinez, E.; Sanchez-Gonzalez, A.; Sordo, J.; Vazquez-Lopez, E. M. *Polyhedron* **2003**, *22*, 1077−1083.

(39) (a) Xu, J.-Y.; Gu, W.; Li, L.; Yan, S.-P.; Cheng, P.; Liao, D.-Z.; Jiang, Z.-H. *J. Mol. Struct.* **2003**, *644*, 23−27. (b) Angulo-Cornejo, J.; Lino-Pacheco, M.; Richter, R.; Hennig, L.; Hallmeier, K.-H.; Beyer, L. *Inorg. Chim. Acta* **2000**, *305*, 38−45. (c) Matthews, C. J.; Heath, S. L.; Elsegood, M. R. J.; Clegg, W.; Leese, T. A.; Lockhart, J. C. *J. Chem. Soc., Dalton Trans.* **1998**, 1973−1978.

(40) Vaiana, L.; Platas-Iglesias, C.; Esteban-Gómez, D.; Avecilla, F.; Clemente-Juan, J. M.; Real, J. A.; de Blas, A.; Rodríguez-Blas, T. *Dalton Trans.* **2005**, 2031−2037.

(41) Gonzalez-Lorenzo, M.; Platas-Iglesias, C.; Avecilla, F.; Geraldes, C. F. G. C.; Imbert, D.; Bünzli, J.-C. G.; de Blas, A.; Rodríguez-Blas, T. *Inorg. Chem.* **2003**, *42*, 6946−6954.

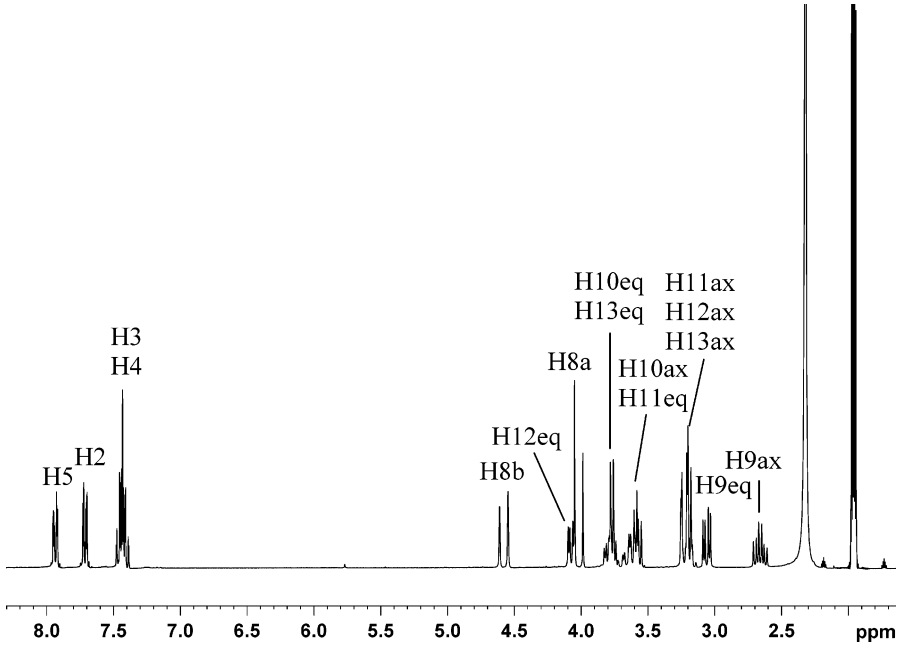

Figure 2. 500 MHz ^{1}H NMR spectrum of the Zn^{II} compound **ZnL^2** as recorded in a CD_3CN solution at 298 K. See Table 4 for labeling.

Table 4. ^{1}H and ^{13}C NMR Shifts (ppm with Respect to TMS) for **ZnL^2** [a]

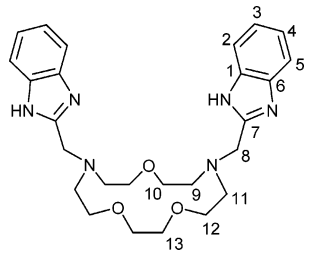

^{1}H	$\delta_{i,exp}$ [a]	^{13}C	$\delta_{i,exp}$ [a]	$\delta_{i,calc}$ [b]	$\delta_{i,calc}$ [c]
H2	7.71 (m, 2H)	C1	136.1	142.1	144.2
H3	7.45 (m, 2H)	C2	114.0	121.3	120.9
H4	7.42 (m, 2H)	C3	125.9	139.3	134.5
H5	7.93 (m, 2H)	C4	125.3	136.7	132.9
H8a	4.02 (d, 2H)	C5	119.6	123.6	126.2
H8b	4.58 (d, 2H)	C6	140.0	145.8	148.2
H9ax	2.66 (td, 2H)	C7	156.5	157.9	163.6
H9eq	3.07 (dd, 2H)	C8	50.3	54.9	55.1
H10ax	3.58 (m, 2H)	C9	55.6	59.7	60.5
H10eq	3.79 (m, 2H)	C10	64.8	70.7	70.8
H11ax	3.23 (m, 2H)	C11	60.6	65.8	66.1
H11eq	3.64 (m, 2H)	C12	66.7	71.5	72.0
H12ax	3.22 (m, 2H)	C13	69.7	74.5	75.0
H12eq	4.08 (dd, 2H)				
H13ax	3.20 (d, 2H)				
H13eq	3.77 (d, 2H)				
NH	11.55 (b, 2H)				

[a] Conditions: Assignment supported by two-dimensional H−H COSY, HMQC, and HMBC experiments at 293 K, CD_3CN, 500 MHz. $^2J_{8a-8b} = {}^2J_{8b-8a} = 18.8$ Hz; $^2J_{12eq-12ax} = 9.9$ Hz; $^3J_{12eq-11ax} = 3.2$ Hz; $^2J_{13eq-13ax} = 6.36$ Hz; $^2J_{9eq-9ax} = 4.8$ Hz; $^3J_{9eq-10ax} = 12.2$ Hz; $^3J_{9ax-10eq} = 6.7$ Hz. [b] Values calculated in vacuo at the B3LYP/6-311G** level by using the GIAO method. [c] Values calculated in an acetonitrile solution at the B3LYP/6-311G** level by using the GIAO method.

experimental values for different coordination compounds,[42] including Zn^{II} complexes.[43] The main results of these calculations together with the experimental values are given in Table 4. Our calculations provide ^{13}C NMR chemical shifts in good agreement with the experimental values, thereby confirming the spectral assignments. These results also indicate that the calculated structure for $[Zn(\mathbf{L^2})]^{2+}$ provides a good model for the structure of the complex in solution. Moreover, the inclusion of solvent effects does not provide a significant improvement between the experimental and calculated ^{13}C NMR shifts (Table 4), highlighting the negligible influence of solvation on the shielding constants of these C atoms. Once the ^{13}C NMR signals were assigned on the basis of the GIAO calculations, a full assignment of the ^{1}H NMR signals was obtained from the cross-peaks observed in the two-dimensional HSQC experiment.

The room-temperature absorption spectra of the five compounds recorded in an acetonitrile solution at 298 K show two absorption maxima at 278 and 272 nm assigned to $\pi^* \leftarrow \pi$ singlet−singlet transitions centered in the benzimidazole units[44] ($^1L_a \leftarrow S_0$ and $^1L_b \leftarrow S_0$, where the two excited states are labeled by ^1L_a and ^1L_b following the suggestion of Platt).[45] The spectrum of the Cu^{II} complex also exhibits a broad and intense absorption overlapping with the ligand $\pi^* \leftarrow \pi$ transitions and extending until ca. 450 nm (Figure 3). This absorption band is not observed in the case of the Mn^{II}, Co^{II}, Ni^{II}, or Zn^{II} complexes, and it is assigned as a charge-transfer (CT) transition.[46] Likewise, this spectrum also shows a weak absorption band envelope between 750 and 2000 nm (<100 M^{-1} cm^{-1}), with three maxima at 1337,

(42) (a) Platas-Iglesias, C.; Mato-Iglesias, M.; Djanashvili, K.; Muller, R. N.; Vander Elst, L.; Peters, J. A.; de Blas, A.; Rodríguez-Blas, T. *Chem.—Eur. J.* **2004**, *10*, 3579−3590. (b) González-Lorenzo, M.; Platas-Iglesias, C.; Avecilla, F.; Faulkner, S.; Pope, S. J. A.; de Blas, A.; Rodríguez-Blas, T. *Inorg. Chem.* **2005**, *44*, 4254−4262.
(43) Panda, M.; Phuan, P.-W.; Kozlowski, M. C. *Chem. Commun.* **2002**, 1552−1553.
(44) Berden, G.; Meerts, W. L.; Jalviste, E. *J. Chem. Phys.* **1995**, *103*, 9596−9606.
(45) Platt, J. R. *J. Chem. Phys.* **1951**, *19*, 101−118.
(46) (a) Auerbach, U.; Eckert, U.; Wieghardt, K.; Nuber, B.; Weiss, J. *Inorg. Chem.* **1990**, *29*, 938−944. (b) Ma, S.-L.; Zhu, W.-X.; Qi, C.-M.; Guo, Q.-L.; Zhang, J.; Liu, Y.-C.; Xu, M.-Q. *J. Mol. Struct.* **2004**, *703*, 25−29.

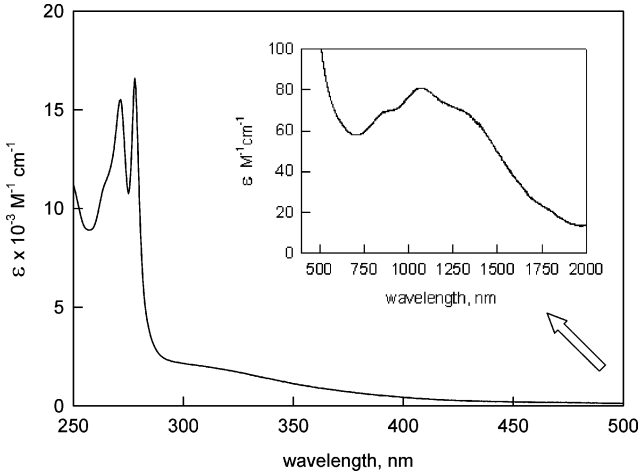

Figure 3. UV−vis spectrum of **CuL²** as recorded in a CH_3CN solution at room temperature.

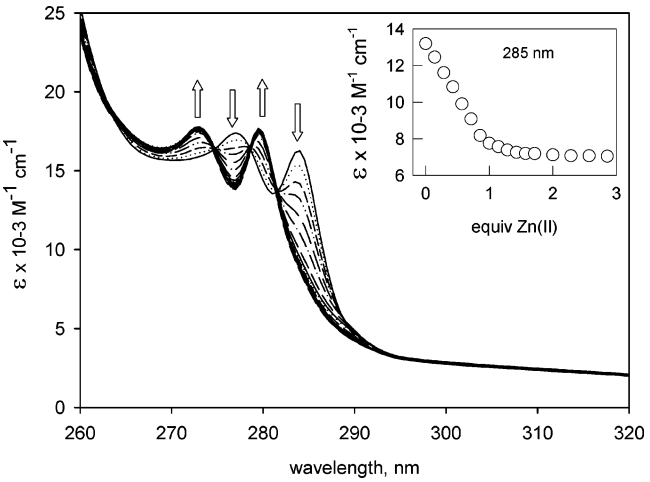

Figure 4. Selected range of the UV−vis spectrum of **L²** in a CH_3CN/DMSO (9:1) mixture and spectral changes upon the addition of aliquots of a solution of $Zn(ClO_4)_2 \cdot 6H_2O$ in the same solvent.

1090, and 886 nm, assigned to d → d transitions (Figure 3), whereas the spectrum of the Ni^{II} complex shows two bands due to d → d transitions: one broad band extending from 930 to 1325 nm, with a maximum at ca. 1050 nm, and another centered at 590 nm, respectively, assigned to the $^3A_{2g}$-(F) → $^3T_{2g}$(F) and $^3A_{2g}$(F) → $^3T_{1g}$(F) transitions in Ni^{II} octahedral complexes. On the other hand, neither the spectrum of the Co^{II} complex nor the one of Mn^{II} shows significant absorption in the 400−1500 nm region, the former probably because the expected absorptions are too weak to be detected at the maximum concentration attainable in an acetonitrile solution (ca. 10^{-2} M) and the latter because the d → d transitions are both spin- and Laporte-forbidden in high-spin d^5 Mn^{II} complexes.

Spectrophotometric Titrations. The coordination of **L²** to Mn^{II}, Co^{II}, Ni^{II}, Cu^{II}, and Zn^{II} was studied by means of spectrophotometric titrations in DMSO and CH_3CN/DMSO (9:1) mixtures (Figure 4). Upon the addition of cobalt(II), nickel(II), copper(II), or zinc(II) perchlorate, the bands at 277 and 284 nm present in the spectrum of the uncoordinated ligand **L²** in DMSO shift toward shorter wavelengths as their intensity slightly increases. These spectral changes indicate the coordination of the benzimidazole pendants to the corresponding metal ion and allowed us to monitor the formation of the complexes in solution. In all cases, a 1:1 reaction stoichiometry was ascertained because the data displayed a single inflection point when the metal-to-ligand molar ratio is close to 1, in agreement with the formation of the expected $[M(\mathbf{L^2})]^{2+}$ (M = Co, Ni, Cu, or Zn) complexes. The spectral changes observed during the course of the titration of **L²** with Mn^{II} show a different behavior. In this case, the addition of metal ion causes small changes in the spectrum of the ligand, which suggests that the pendant arms do not coordinate to the Mn^{II} ion in a DMSO solution and prevented us from obtaining an experimental value for the formation constant of this complex in DMSO. For the Co^{II}, Ni^{II}, and Zn^{II} complexes, the titration data allowed us to determine binding constants defined as

$$\mathbf{L^2} + M^{2+} \leftrightarrows [M(\mathbf{L^2})]^{2+} \qquad \beta_{11}$$

and the results are compiled in Table 5. In the case of the Cu^{II} complex, further spectral changes were observed upon formation of the 1:1 (M/L) complex, due to the CT absorption band of a DMSO Cu^{II} complex formed, which is centered at 285 nm ($\epsilon = 5761.30 \pm 24.78$ M^{-1} cm^{-1}) and, therefore, a reliable binding constant could not be obtained. In the case of the Co^{II} and Ni^{II} complexes, the steep curvature of the titration profile corresponds to an especially high equilibrium constant. Under this situation, the *p* parameters (p = [concentration of the complex]/[maximum possible concentration of the complex]) take values close to 1, which causes larger errors in the determination of the binding constants.[47] Thus, in order to obtain more accurate formation constants for these complexes, we carried out competitive titration experiments in the presence of 1 equiv of Zn^{II} in CH_3CN/DMSO (9:1). Similar competitive titration experiments also allowed us to obtain a binding constant for Mn^{II}. As expected, the binding constants obtained from competitive titration for the Co^{II} and Ni^{II} complexes show smaller standard deviations than those obtained from direct titrations. The results (Table 5) indicate the following stability sequence for the complexes of **L²**: $Co^{II} \approx Ni^{II} > Zn^{II} \gg Mn^{II}$. The

Table 5. UV−Vis Spectral Data of **L²** and $[M(\mathbf{L^2})]^{2+}$ Complexes and Binding Constants Obtained from Spectrophotometric Titrations at 25 °C

	λ_{max} (nm)[a]	ϵ (10^{-3} M^{-1} cm^{-1})[a]	log β_{11}[a]	log β_{11}[b]
L²	284	17.1		
	276	18.1		
$[Mn(\mathbf{L^2})]^{2+}$ [a]	280	16.5	*c*	2.65(3)[d]
	273	15.8		
$[Co(\mathbf{L^2})]^{2+}$	280	17.2	7.8(8)	7.79(9)[d]
	274	17.4		
$[Ni(\mathbf{L^2})]^{2+}$	280	18.3	7.0(3)	7.70(5)[d]
	274	18.4		
$[Zn(\mathbf{L^2})]^{2+}$	280	17.3	5.78(2)	5.85(2)
	273	17.4		

[a] Data obtained from DMSO solutions. [b] Data obtained from CH_3CN/DMSO (9:1) solutions. [c] The addition of the metal ion causes few spectral changes, preventing the determination of a binding constant. [d] Data obtained from competitive titration experiments.

(47) Wilcox. C. S. *Frontiers in Supramolecular Chemistry and Photochemistry*; VCH: Weinheim, Germany, 1991; pp 123−143.

log β_{11} value determined for the Zn^{II} complex [5.85(2)] is only slightly lower than those reported previously for the Cd^{II} and Pb^{II} analogues in the same conditions (log β_{11} = 6.23 and 6.15, respectively).[20]

Geometry Optimizations. Full geometry optimizations of the $[M(\mathbf{L^2})]^{2+}$systems (M = Mn, Co, Ni, Cu, or Zn) by means of DFT calculations were performed in vacuo by using the standard 6-31G(d) basis set on the ligand atoms and Ahlrichs' VTC on the metal atoms.[27] In a recent paper, we have demonstrated that a similar computational approach provides molecular geometries in good agreement with the solid-state structures of the corresponding mononuclear complexes of the related receptor $\mathbf{L^1}$.[18,19] On the basis of the magnetic properties described above, the spin multiplicity of the Mn, Co, Ni, and Cu centers were fixed at 6, 4, 3, and 2, respectively. The geometry optimizations on the $[Zn(\mathbf{L^2})]^{2+}$ complex were performed by using the restricted B3LYP model, while those corresponding to the other four metal complexes were carried out using the unrestricted B3LYP model. In our calculations, the two different conformations observed in the solid state for $\mathbf{NiL^2}$ and $\mathbf{ZnL^2}$ (with the octahedral and pentagonal-bipyramidal coordination polyhedra, respectively) were considered. Attempts to model the octahedral coordination on the Mn, Co, Cu, and Zn complexes lead systematically to the seven-coordinated geometry during the optimization process. However, for $[Ni(\mathbf{L^2})]^{2+}$, two minimun-energy conformations with pentagonal-bipyramidal (denoted as *pb*-$[Ni(\mathbf{L^2})]^{2+}$) and octahedral (labeled as *o*-$[Ni(\mathbf{L^2})]^{2+}$) coordination environments have been obtained. Tables 2 and 3 show calculated bond distances and angles of the metal coordination environments for the different $[M(\mathbf{L^2})]^{2+}$ systems. The calculated structures of the corresponding *pb*-$[M(\mathbf{L^2})]^{2+}$ complexes show nearly undistorted C_2 symmetries, with the symmetry axis containing one of the O atoms of the crown moiety (O3) and the metal ion. According to Table 2, the bond lengths calculated for $[Zn(\mathbf{L^2})]^{2+}$ are close to those observed experimentally (within 0.10 Å), as evidenced by the excellent agreement factor obtained $AF_i = 0.027$ ($AF_i = [\sum(\text{exp} - \text{calcd})^2/\sum(\text{exp})^2]^{1/2}$, where exp and calcd denote calculated and experimental values, respectively).[48] The experimental and calculated bond angles of the metal coordination environment also show a good agreement ($AF_i = 0.027$; Table 2). These agreement factors take values similar to those found previously for complexes $[M(\mathbf{L^1})]^{2+}$ (M = Mn, Co, or Zn).[18,19] The M−N2 and M−N6 bond distances in these pentagonal-bipyramidal complexes gradually decrease from Mn to Cu and then increase for $[Zn(\mathbf{L^2})]^{2+}$, while the bond distances to donor atoms of the crown moiety show a more complicated variation along the first-row transition-metal series that marks important changes in the metal−ligand bonding depending on the electronic configuration of the metal ion. On the other hand, the calculated bond distances and angles of the metal coordination environment in *o*-$[Ni(\mathbf{L^2})]^{2+}$ also show a reasonably good agreement with those observed in the solid state (within 0.09 Å; Table 3), with agreement factors AF_i = 0.021 and 0.013 for bond distances and angles, respectively.

Discussion

Seven-coordination is a quite infrequent coordination number for divalent first-row transition metals, and it has an irregular distribution along this series, being by far less common for Ni than for the other elements.[4] We have reported that the biarmed heptadentate receptor $\mathbf{L^1}$ is able to impose a pentagonal-bipyramidal geometry not only on Mn, Co, Cu, and Zn but also on Ni.[17−19] However, the data presented here under the Results section show that the also heptadentate receptor $\mathbf{L^2}$ ′only forces such a coordination geometry in the case of Mn^{II}, Co^{II}, Cu^{II}, and Zn^{II} complexes but not for Ni^{II}. Both receptors are structurally related, but $\mathbf{L^2}$ contains benzimidazol-2-ylmethyl pendant arms able form five-membered chelate rings upon coordination to the metal ion, while the 2-aminobenzyl pendants of $\mathbf{L^1}$ form six-membered chelate rings. Aiming to rationalize these experimental results, we have performed a study of the electronic structure on the $[M(\mathbf{L^2})]^{2+}$ systems (M = Mn, Co, Ni, Cu, or Zn) at the DFT (B3LYP) computational level, as well as MO analysis. In order to simplify the study of the electronic structure, it is convenient to define a local coordinate system that will apply for the $[M(\mathbf{L^2})]^{2+}$ complexes. The coordinate system chosen together with a quantitative MO diagram for the different $[M(\mathbf{L^2})]^{2+}$ systems is shown in Figure 5. Spin-unrestricted calculations give different absolute energies for α ("up") and β ("down") spin orbitals because of the different number of electrons in each spin state. The energies shown in Figure 5 are for the β spin orbitals containing important metal character. Other orbitals are omitted for simplicity. Contour surfaces of the β MOs with important 3d metal character in *pb*-$[Co(\mathbf{L^2})]^{+2}$ are shown in Figure S2 (Supporting Information). The orbital labels follow the usual convention for symmetry labels in C_2, except that the numbering is arbitrarily begun with the lowest energy state shown. The energies and occupancies of the frontier β MO with important metal character, together with the contributions of atomic 3d orbitals of the metal calculated by Mulliken population analysis (MPA),[49] are listed in Table 6. As can be seen from the MO energy diagram shown in Figure 5, the metal β 3d orbitals decrease in energy when proceeding from left to the right across the first-row transition-metal series. This is mainly due to the relative nuclear charge of the metal ions. The Mn^{II}, Co^{II}, and Cu^{II} pentagonal-bipyramidal complexes show an identical ordering of the metal-based frontier MOs that agrees with the qualitative view for a pentagonal-bipyramidal molecular coordination presented by Hoffman et al.[10] on the basis of extended Hückel calculations. The metal contribution to the first two β frontier MOs, $a^{(1)}$ and $b^{(1)}$, which are correlated with the double-degenerate e_1'' orbitals in D_{5h} symmetry, is mainly d_{yz} and d_{xz}, respectively (Table 6). At somewhat higher energy are the $a^{(2)}$ and $b^{(2)}$ MOs, which are related to

(48) (a) Willcott, M. R.; Lenkinski, R. E.; Davis, R. E. *J. Am. Chem. Soc.* **1972**, *94*, 1742−1744. (b) Davis, R. E.; Willcott, M. R. *J. Am. Chem. Soc.* **1972**, *94*, 1744−1745.

(49) Mulliken, R. S. *J. Chem. Phys.* **1955**, *23*, 1833−1840.

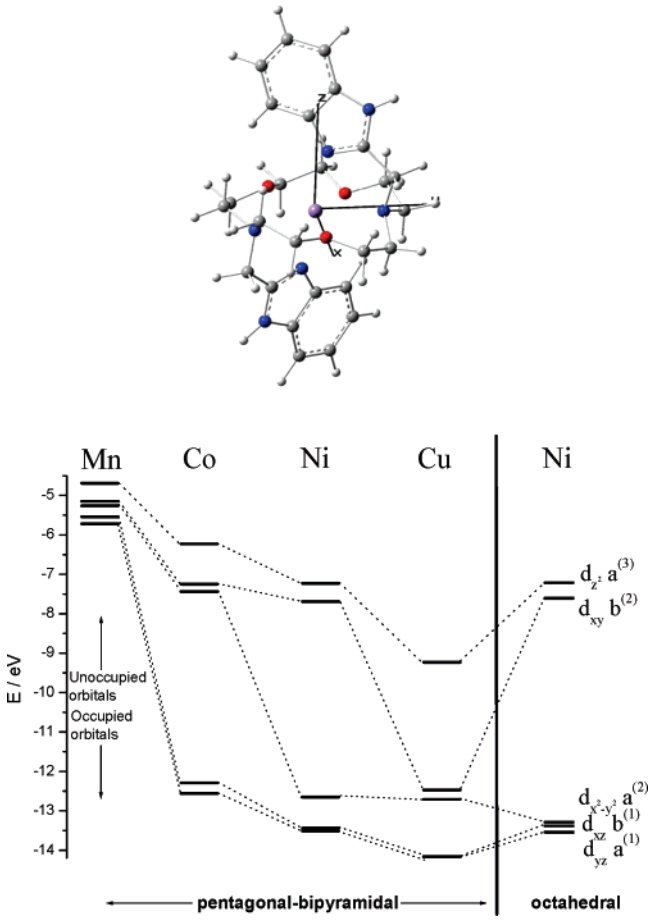

Figure 5. Top: Definition of the coordinate system for the $[M(\mathbf{L^2})]^{2+}$ complexes used in electronic structure calculations. Bottom: β-Spin frontier MOs of the $[M(\mathbf{L^2})]^{2+}$ complexes (M = Mn, Co, Ni, or Cu) with important 3d metal character.

the double-degenerate e_2' orbitals in D_{5h} symmetry and possess $d_{x^2-y^2}$ and d_{xy} character, respectively (Table 6). At highest energy are the $a^{(3)}$ orbitals, whose metal contribution is primarily d_{z^2} (Table 6).

In the *pb*-$[Mn(\mathbf{L^2})]^{2+}$ complex, all of the β-spin 3d orbitals of the central atom are unoccupied, while in the Co^{II} complex, with two more valence electrons, the $a^{(1)}$ and $b^{(1)}$ orbitals become occupied, being stabilized by ca. 6.8 eV relative to the analogous orbitals in the Mn complex. Surface plots suggest a π-antibonding character of the $b^{(1)}$ MO with respect to the interaction between the metal and the O atoms of the ligand. This is confirmed by the calculated ODOS values (Table 6), which shows a negative value for this MO with respect to the metal−ligand interaction. ODOS values provide information about the bonding, nonbonding, or antibonding character of MOs with respect to particular molecular fragments. A positive ODOS value represents a bonding situation, a negative value represents an antibonding one, and a value close to zero indicates no bonding between the molecular fragments.[50] Surface plots also show that the $a^{(1)}$ MO is antibonding with respect to the interaction between the metal and the O atoms of the macrocyclic receptor. This

(50) Ghosh, S.; Gorelsky, S. I.; Chen, P.; Cabrito, I.; Moura, J. J. G.; Moura, I.; Solomon, E. I. *J. Am. Chem. Soc.* **2003**, *125*, 15708−15709.

Table 6. Irreducible Representations, Energies, and Occupancies of the Frontier β MO As Obtained from UB3LYP Calculations for the $[M(\mathbf{L^2})]^{2+}$ Complexes (M = Mn, Co, Ni, or Cu), Contributions of the 3d Atomic Orbital of the Metal (Obtained by MPA), and ODOS Values

M	$\Gamma(C_2)$	energy/eV	occ	% 3d	ODOS[a]
$[Mn(\mathbf{L^2})]^{2+}$	$a^{(3)}$	−4.69	0	49.2 d_{z^2}	−0.108
	$b^{(2)}$	−5.15	0	87.4 d_{xy}	−0.055
	$a^{(2)}$	−5.26	0	83.0 $d_{x^2-y^2}$	−0.048
	$b^{(1)}$	−5.54	0	58.1 d_{xz}	−0.010
	$a^{(1)}$	−5.72	0	42.4 d_{yz}	−0.065
$[Co(\mathbf{L^2})]^{2+}$	$a^{(3)}$	−6.23	0	76.5 d_{z^2}	−0.128
	$b^{(2)}$	−7.25	0	66.7 d_{xy}	−0.047
	$a^{(2)}$	−7.44	0	72.4 $d_{x^2-y^2}$	−0.040
	$b^{(1)}$	−12.29	1	50.8 d_{xz}	−0.031
	$a^{(1)}$	−12.56	1	63.0 d_{yz}	−0.022
bp-$[Ni(\mathbf{L^2})]^{2+}$	$a^{(3)}$	−7.23	0	75.7 d_{z^2}	−0.145
	$b^{(2)}$	−7.69	0	85.4 d_{xy}	−0.085
	$a^{(2)}$	−12.65	1	23.6 $d_{x^2-y^2}$	−0.030
	$b^{(1)}$	−13.44	1	32.5 d_{xz}	−0.014
	$a^{(1)}$	−13.51	1	49.4 d_{yz}	−0.031
o-$[Ni(\mathbf{L^2})]^{2+}$	$a^{(3)}$	−7.22	0	75.2 d_{z^2}	−0.646
	$b^{(2)}$	−7.61	0	67.7 d_{xy}	−0.406
	$a^{(2)}$	−13.29	1	22.0 $d_{x^2-y^2}$	−0.163
	$b^{(1)}$	−13.38	1	48.1 d_{xz}	−0.083
	$a^{(1)}$	−13.54	1	49.3 d_{yz}	−0.112
$[Cu(\mathbf{L^2})]^{2+}$	$a^{(3)}$	−9.23	0	60.1 d_{z^2}	−0.171
	$b^{(2)}$	−12.47	1	17.2 d_{xy}	−0.063
	$a^{(2)}$	−12.71	1	14.5 $d_{x^2-y^2}$, 3.8 d_{z^2}	−0.035
	$b^{(1)}$	−14.16	1	18.9 d_{xz}	−0.033
	$a^{(1)}$	−14.22	1	3.9 d_{yz}	−0.009

[a] The ODOS values were calculated by considering the interaction between the ligand and metallic center.

is again confirmed by the corresponding ODOS value (Table 6). Because of the occupation of $a^{(1)}$ and $b^{(1)}$, both antibonding with respect to the M−O interactions, the M−O1 and M−O2 distances are only slightly shorter in the *pb*-$[Co(\mathbf{L^2})]^{2+}$ complex when compared to the Mn^{II} analogue, while the M−O3 bond distance is longer in *pb*-$[Co(\mathbf{L^2})]^{2+}$ (Table 2). In the *pb*-$[Ni(\mathbf{L^2})]^{+2}$ complex, with one more valence electron than the Co^{II} one, the $a^{(2)}$ MO becomes occupied, and it is stabilized by 5.21 eV relative to the analogous orbital in the Co complex. The $a^{(2)}$ MO possesses antibonding character with respect to the interaction between the metal ion and the ligand (Table 6). The occupation of this antibonding orbital weakens the metal−donor bonds directing to the extent of the orbitals. Indeed, $a^{(2)}$ possesses a strong antibonding character with respect to the interaction with O3, N3 and N4, which results in the lengthening of the calculated Ni−O3, Ni−N3, and Ni−N4 bond distances (Table 2) when compared to those calculated for the Co analogue. The *o*-$[Ni(\mathbf{L^2})]^{2+}$ complex shows an ordering of the metal-based frontier MOs that is similar to that calculated for the *pb*-$[Ni(\mathbf{L^2})]^{2+}$ form, with the main difference being the stabilization of the occupied $a^{(2)}$ MO by 0.64 eV in the octahedral form (Table 6 and Figure 5).

In *pb*-$[Cu(\mathbf{L^2})]^{2+}$, the next d orbital (d_{xy}) becomes occupied. This orbital is antibonding with respect to the interaction of the metal and most of the donor atoms of the crown moiety. The occupation of the antibonding $a^{(2)}$ and $b^{(2)}$ MOs weakens the interaction between the metal ion and the donor atoms of the crown moiety. As a result, the corresponding bond distances are longer in the Cu complex than in the Co one in spite of the higher effective nuclear charge of the metal ion in the first complex. On the other hand, in the Zn

complex, the $a^{(3)}$ orbital, which is strongly antibonding with respect to the interaction between the metal ion and the donor atoms of the pendant arms, becomes occupied. As a result, the calculated M−N2 and M−N6 bond distances are longer in this complex than in the Cu one. In $[Zn(\mathbf{L^2})]^{2+}$, all of the d orbitals of the metal ion are occupied, and the covalent bonding interactions between the Zn 3d orbitals and the ligand orbitals are cancelled, which also explains the lower stability of the Zn complex when compared to those of Co and Ni (vide supra).

It is well-known that the half-filled $3d^5$ (high-spin) or filled $3d^{10}$ shells of the Mn^{II} and Zn^{II} ions make them behave as spherically polarizable ions, with no crystal-field stabilization energy. Therefore, there are no electronic restraints, and the structures of the Mn^{II} and Zn^{II} complexes are those that minimize the sterical repulsion. Thus, it is not surprising that the geometry optimizations of the $[Mn(\mathbf{L^2})]^{2+}$ and $[Zn(\mathbf{L^2})]^{2+}$ complexes give systematically pentagonal-bipyramidal coordination environments for these complexes. A similar behavior is observed for the Cu^{II} complex, for which geometry optimizations lead also to a pentagonal-bipyramidal coordination. This is attributed to the fact that the $a^{(2)}$ and $b^{(2)}$ frontier MOs become occupied in this complex and the seventh donor atom (O3) is placed on the *xy* plane, so that there is no electronic preference for the octahedral or pentagonal-bipyramidal coordination. However, the situation is different for the Ni^{II} complex, for which both octahedral and pentagonal-bipyramidal geometries could be modeled by using DFT calculations. From the calculated structure of the *pb*-$[Ni(\mathbf{L^2})]^{2+}$ system (Table 2), it follows that two of the Ni−O distances of the metal coordination environment (Ni1−O1 and Ni1−O2) are clearly shorter than those observed for the other complexes, while the Ni1−O3 distance is clearly longer than the M−O3 distances calculated for the remaining *pb*-$[M(\mathbf{L^2})]^{2+}$ systems. This distortion of the Ni^{II} coordination environment is attributed to the Jahn−Teller effect, which is expected to operate in seven-coordinated pentagonal-bipyramidal Ni^{II} complexes.[51] In the calculated geometry of *o*-$[Ni(\mathbf{L^2})]^{2+}$, the Ni−O3 distance is so long that it cannot be considered as a bond distance (3.16 Å). Thus, the octahedral geometry in the Ni^{II} complex can be considered as the result of the Jahn−Teller effect operating in pentagonal-bipyramidal Ni^{II} complexes, which in an extreme case leads to an octahedral geometry. Aiming to better understand the reasons responsible for a heptadentate ligand giving seven or six Ni^{II} coordination, we have also tried to model an octahedral coordination environment in $[Ni(\mathbf{L^1})]^{2+}$ by using B3LYP calculations. However, geometry optimizations lead systematically to a pentagonal-bipyramidal coordination environment. A comparison between receptors $\mathbf{L^1}$ and $\mathbf{L^2}$ (Chart 1) shows that whereas $\mathbf{L^1}$ contains 2-aminobenzyl pendant arms that give six-membered chelate rings upon coordination to the metal ion, $\mathbf{L^2}$ possesses benzimidazol-2-ylmethyl pendants that form five-membered chelate rings. Thus, our calculations suggest that the size of the chelate rings formed upon coordination of the pendant arms in Ni^{II} complexes with heptadentate ligands derived from the 1,10-diaza-15-crown-5 moiety may have an influence on the coordination number (six vs seven) around this metal ion, although the different nature of the donor atoms of the pendant arms in $\mathbf{L^1}$ and $\mathbf{L^2}$ may also have an influence on the metal coordination environment.

(51) Giordano, T. J.; Palenik, G. L.; Palenik, R. C.; Sullivan, D. A. *Inorg. Chem.* **1979**, *9*, 2445−2450.

Table 7. Selected TDDFT-Calculated Excitation Energies and Compositions of the Lowest-Lying Excited States for $[Cu(\mathbf{L^2})]^{2+}$ and Experimental UV−Vis Absorption Data Obtained in an Acetonitrile Solution at 25 °C

state	ΔE/eV	λ_{calcd}/nm	f	λ_{exp}/nm[a]	assignment
1	0.90	1375	0.0012	1337	$b^{(2)} \rightarrow a^{(3)}$ (39%)
2	1.11	1117	0.0008	1090	$a^{(2)} \rightarrow a^{(3)}$ (29%)
3	1.44	863	0.0002	886	$b^{(1)} \rightarrow a^{(3)}$ (22%)

[a] Data obtained from a 10^{-2} M solution of the complex in CH_3CN.

TDDFT calculations performed on the *pb*-$[Cu(\mathbf{L^2})]^{+2}$ system have been used to investigate the electronic spectrum of the Cu complex. Table 7 shows a comparison between the calculated excited-state energies and oscillator strengths (f) relevant to the interpretation of the electronic spectra in the region 500−2000 nm. The calculated first three low-energy bands are in a nice agreement with the experimental data (Table 7). The largest contribution (ca. 39%) to the first calculated electronic transition at 1375 nm is the excitation from the β MO $b^{(2)}$ into the β lowest unoccupied MO $a^{(3)}$ (Figure 5). The following calculated electronic transition at 1117 nm is primarily the result of an $a^{(2)} \rightarrow a^{(3)}$ excitation, while the third calculated electronic transition at 863 nm presents an important contribution of the $b^{(1)} \rightarrow a^{(3)}$ excitation (Table 7). Thus, our TDDFT calculations allow us to assign the first three electronic transitions observed for the $[Cu(\mathbf{L^2})]^{2+}$ complex as ligand-field (LF) transitions in the following order: $d_{xy} < d_{x^2-y^2} < d_{xz}$. Moreover, the excellent agreement between the experimental and calculated LF transitions clearly confirms that the Cu^{II} complex adopts in solution a *pb*-$[Cu(\mathbf{L^2})]^{2+}$ geometry.

Conclusions

The heptadentate receptor $\mathbf{L^2}$ forms mononuclear complexes of the formula $[M(\mathbf{L^2})](ClO_4)_2$ with Mn^{II}, Co^{II}, Ni^{II}, Cu^{II}, and Zn^{II}. Unlike what happens with the related receptor $\mathbf{L^1}$ containing 2-aminobenzyl pendant arms, for which all of the corresponding complexes are seven-coordinated with a pentagonal-bipyramidal environment around the metal ion,[17−19] in $[M(\mathbf{L^2})]^{2+}$ some important structural differences are found. As expected, the X-ray crystal structure of the Zn^{II} complex shows the metal ion in a distorted pentagonal-bipyramidal coordination environment bound to the seven donor atoms of the receptor, while the corresponding structure of the Ni^{II} complex shows the Ni ion being only six-coordinated in a distorted octahedral coordination environment. Geometry optimizations on the $[M(\mathbf{L^2})]^{2+}$ (Mn, Co, Cu, and Zn) complexes lead systematically to the seven-coordinated geometry during the optimization process. However, for $[Ni(\mathbf{L^2})]^{2+}$, two minimun-energy conformations with pentagonal-bipyramidal (*pb*-$[Ni(\mathbf{L^2})]^{2+}$) and octahedral (*o*-$[Ni(\mathbf{L^2})]^{2+}$) coordination environments were obtained. The variation of the bond distances of the metal coordination

environment along the first-row transition-metal series can be rationalized on the basis of the different occupations of the frontier MOs with important metal character depending on the electronic configuration of the metal ion. Moreover, the octahedral geometry found in the Ni^{II} complex can be considered as the result of the Jahn−Teller effect operating in pentagonal-bipyramidal Ni^{II} complexes, which in an extreme case leads to an octahedral geometry. These results are in agreement with a recent estimate based on the number of first-row transition-metal σ-bonded complexes found in the Cambridge Structural Database, which reveals that seven-coordination is by far less common for Ni than for Mn, Fe, and Co and even Cu or Zn.[4]

Spectrophotometric titrations indicate the following stability sequence for the complexes of $\mathbf{L^2}$: $Co^{II} \approx Ni^{II} > Zn^{II} \gg Mn^{II}$. Finally, the data here reported have also proved that TDDFT calculations are able to predict rather accurately the absorption spectrum of the pentagonal-pipyramidal Cu^{II} complex.

Acknowledgment. Authors thank Xunta de Galicia (Grant PGIDIT06TAM10301PR) and Universidade da Coruña for generous financial support. The authors are indebted to Centro de Supercomputación de Galicia (CESGA) for providing the computer facilities. They also thank Prof. J. A. Real (University of Valencia, Valencia, Spain) for useful help in the analysis of the magnetic data.

Supporting Information Available: X-ray crystallographic files in CIF format for compounds $\mathbf{NiL^2}$ and $\mathbf{ZnL^2}$, difference between ideal and actual spin (spin contamination, Table S1), plots of $\chi_M T$ vs T for compounds $\mathbf{ML^2}$ (M = Mn, Co, Ni, or Cu; Figure S1), surface plots of the Co-based β MOs obtained from UB3LYP calculations for $[Co(\mathbf{L^2})]^{2+}$ (Figure S2), and in vacuo optimized Cartesian coordinates (Å) for the $[M(\mathbf{L^2})]^{2+}$ systems (M = Mn, Co, Ni, Cu, or Zn). This material is available free of charge via the Internet at http://pubs.acs.org.

IC7008946